Available online at www.eccomasproceedia.org
Eccomas Proceedia EUROGEN (2023) 132-145

ECCOMAS
Proceedia

EUROGEN 2023
15th ECCOMAS Thematic Conference on
Evolutionary and Deterministic Methods for Design, Optimization and Control
N. Gauger, K. Giannakoglou, M. Papadrakakis, J. Periaux (eds.)
Chania, Crete Greece, 1–3 June 2023

# MULTI-OBJECTIVE OPTIMIZATION OF LIQUID STORAGE TANKS WITH HYBRID ISOLATION SYSTEM

**Alexandros Tsipianitis**[1] **& Yiannis Tsompanakis**[2]

[1] Research Associate, Computational Dynamics & Energy Laboratory (CODEN), School of Chemical & Environmental Engineering, Technical University of Crete
University Campus, 73100, Chania, Greece
e-mail: atsipianitis@tuc.gr

[2] Professor, Head of Computational Dynamics & Energy Laboratory (CODEN), School of Chemical & Environmental Engineering, Technical University of Crete
University Campus, 73100, Chania, Greece
e-mail: jt@science.tuc.gr

## Abstract

*Liquid storage tanks have proven to be efficiently protected by seismic isolation schemes, which manage to reduce the distress of the superstructure. However, strong pulse-like ground motions generated by near-fault earthquakes can impose excessive displacement demands on the isolators of tanks located in seismic-prone areas. An efficient solution to this problem is the adoption of a hybrid system, i.e., elastomeric or friction-based isolators with supplemental passive energy dissipation devices. The application of multi-objective optimization approaches is suitable for such problems that require to include and handle simultaneously several competing objectives, which can be significantly different (i.e., related to time, cost, performance, etc.). In particular, the combination of single friction pendulum bearings and linear viscous dampers is a case that requires the consideration of many design objectives and constraints. Therefore, the main aim of this work is to optimize the critical design parameters by achieving a reasonable balance among contradicting objectives. The multi-objective genetic algorithm (MOGA) optimizer will be used for the solution of two optimization problems. The results are presented in the typical form of two-dimensional, as well as three-dimensional Pareto fronts, while certain optimal design solutions are selected and compared in terms of isolators' fragility curves and tank accelerations.*

**Keywords:** Multi-Objective Optimization, Liquid Storage Tanks, Seismic Isolation, Seismic Vulnerability.


Peer-review under responsibility of the organizing committee of EUROGEN 2023.
doi: 10.7712/140123.10195.18959

## 1 INTRODUCTION

Large-scale liquid storage tanks constitute very important infrastructure, as they are widely used to safely store and deliver the content of hazardous chemicals and liquids (e.g., water, oil, liquefied natural gas). However, in previous earthquakes, such as Northridge (1994), Kobe (1995), and Chi-Chi (1999), leakages, explosions and tank wall damages have been observed in liquid storage tanks. In general, significant socioeconomic losses, as well as severe environmental problems may result from such failures. Consequently, the maintenance of their structural integrity in severe earthquakes should be ensured via an efficient seismic design and efficient protection methods.

Base-isolation technology has proven to be an efficient approach to reduce the probability of failure of liquid storage tanks [1]. Due to the low horizontal and high vertical flexibility of the isolators, although the displacements are increased, while the superstructure's acceleration and stresses are notably reduced. However, the displacement demands may be significantly increased when the structure is located in near-fault areas. Two possible solutions can be proposed for the solution of this problem: (a) by selecting isolation devices with large displacement capacity (leading to an overconservative and expensive design), or (b) by adding dampers (e.g., viscous, friction, etc.) at the base-isolation system [2]. Therefore, if the hybrid system is properly designed, an improved seismic performance can be achieved using the latter approach.

Some relevant studies have examined the multi-objective optimization of the seismic response of other type of structures and storage tanks isolated by solely isolators or hybrid systems. Pourzeynali and Zarif [3] applied multi-objective genetic algorithms (MOGA) to optimize base-isolated high-rise buildings. In particular, the main parameters of isolators were optimized via non-dominated sorting genetic algorithm (NSGA-II) to minimize the superstructure and isolators' displacements. Ozbulut et al. [4] also used a MOGA for the learning process of an adaptive neural controller. The scope of this work was to study the adaptive control of structures isolated by a hybrid system, consisting of laminated rubber bearings and variable friction dampers (VFD).

Fallah and Zamiri [5] implemented NSGA-II multi-objective optimization scheme to investigate the seismic response of base-isolated buildings. According to the presented results, the optimum values of isolator properties contributed to the substantial improvement of superstructure's response. In addition, it was reported that the response of the base-isolated system can be improved by the addition of viscous dampers. Labaf et al. [6] examined the multi-objective optimal design of a hybrid control system that consisted of a base isolation system and a tuned mass damper inerter for the seismic protection of liquid storage tanks. It was shown that impulsive and convective displacements, as well as base shear force were reduced more than 80% due to the optimal design of the hybrid isolation system.

In the current investigation, two multi-objective optimization approaches are implemented, consisting of three and four objective functions respectively, as well as suitable constraint functions and design variables to deal efficiently with the problem at hand. More specifically, the constraint functions are related to isolated system's damping and period, while the design variables are the friction coefficient, the radius of curvature of isolators and the damping coefficient of supplemental viscous dampers [9]. Both formulations utilize the multi-objective genetic algorithm optimizer, while the results are presented in the form of two-dimensional and three-dimensional Pareto fronts. The main aim is to optimize of critical design parameters of the coupled system by achieving a reasonable balance among contradicting objectives in terms of performance and cost.

## 2 BASE-ISOLATED LIQUID STORAGE TANKS

As aforementioned, the application of base-isolation systems in liquid storage tanks has led to the efficient reduction of their seismic distress. However, the numerical modeling of the dynamic performance of base-isolated storage tanks is a complex and challenging task. Moreover, it requires a substantial computational effort, especially if the coupled system is simulated utilizing detailed 3-D numerical models. For this purpose, the surrogate model initially developed by Bakalis et al. [7] for fixed-base tanks has been used in this work, as relevant studies in the literature (e.g., Guler and Alhan [8]) have proven that simplified models can be efficiently used for the dynamic analysis of base-isolated tanks. In this study, two tank geometries are examined, i.e., a squat tank with slenderness ratio equal to $H/R$=0.67 and a slender tank with $H/R$=3. The properties and the implementation of the adopted surrogate models are described in authors' recent work [9].

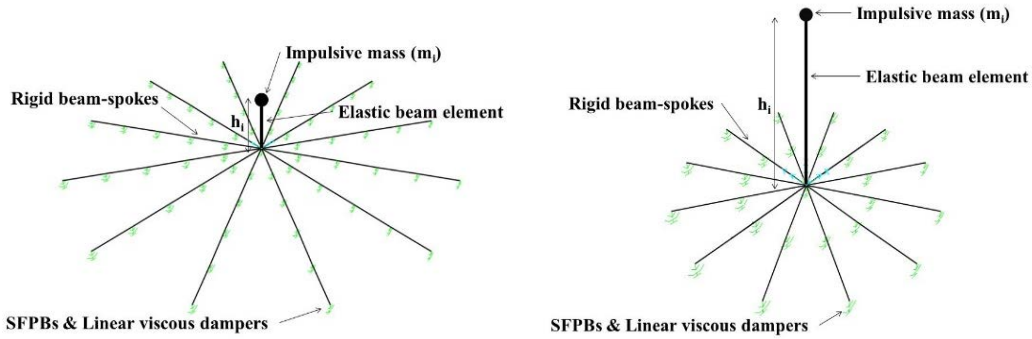


Figure 1: Numerical models with hybrid isolation of (a) the squat and (b) slender tank.

As shown in Figure 1, the surrogate model of each tank consists of a beam-column element that carries the impulsive mass of the tank. It is supported by rigid beam-spokes, which in turn are supported by the hybrid isolation system. The combined base-isolation system consists of single friction pendulum bearings (SFPB) and linear viscous dampers. This scheme provides an effective way to seismically protect buildings of high importance (e.g., museums, hospitals) and other infrastructure (e.g., bridges, liquid storage tanks). In general, the main aim of the application of supplemental dampers is: (a) to reduce the isolators' displacement demand, which is increased when the structures are located in near-fault areas, (b) to minimize the superstructure accelerations, and (c) to achieve a more cost-efficient design of the isolation system.

An iterative approach is utilized for the determination of isolation system parameters (e.g., effective stiffness, $K_{eff}$, effective damping, $\beta_{eff}$, etc.) for a certain friction coefficient, $\mu$, and radius of curvature, $R$, for 61 and 25 SFPB devices installed at the squat and slender storage tank, respectively. For the design of hybrid-isolated storage tanks, the equivalent linear force (ELF) procedure is used following the recommendations of Eurocode 8 (Soil A, $\gamma_I$=1.6, $a_g$=0.36g). In addition, viscous dampers are placed in parallel with the isolators, i.e., equal number of isolators and viscous dampers are applied, based on engineering practice (e.g., Lafontaine et al. [10]). The damper coefficient, $c$, for each damper is derived by [11]:

$$n \cdot c = 2 \cdot \zeta \cdot \omega \cdot m = 2 \cdot \zeta \sqrt{\frac{n \cdot k_{isol}}{m}} \cdot m \Rightarrow c = \frac{2\zeta\sqrt{n \cdot k_{isol} \cdot m}}{n} \quad (1)$$

where $n$ is the number of SFPB isolators, $\zeta$ is the percentage of supplemental damping [%], $k_{isol}$ is the isolator stiffness [N/m], and $m$ is the liquid mass [kg]. According to Taylor [12], the vertical stiffness of the dampers is quite high.

## 3 DYNAMIC ANALYSIS AND EARTHQUAKE SELECTION

The two storage tanks supported on SFPB isolators and linear viscous dampers are modeled utilizing SAP2000 structural analysis software [13]. In addition, the Application Programming Interface (API) provided by SAP2000 is combined with MATLAB software [14]. In this manner, all required steps for the dynamic analyses (e.g., surrogate modeling, ground motion scaling, processing of the results, etc.) can be efficiently performed. Table 1 lists the twenty ground motions taken from the near-fault database of FEMA/SAC Steel project (https://nisee.berkeley.edu/elibrary/files/documents/data/strong_motion/sacsteel/motions/nearfault.html). This set is used to test the hybrid isolation system under large-pulse excitations.

| No | SAC Ref | Record | Moment Magnitude | Distance (km) | PGA (g) | PGV (m/s) |
|---|---|---|---|---|---|---|
| #1 | NF01 | Tabas, 1978 | 7.4 | 1.2 | 0.90 | 1.13 |
| #2 | NF03 | Loma Prieta, 1989, Los Gatos | 7 | 3.5 | 0.72 | 1.36 |
| #3 | NF05 | Loma Prieta, 1989, Lex. Dam | 7 | 6.3 | 0.69 | 1.54 |
| #4 | NF07 | C. Mendocino, 1992, Petrolia | 7.1 | 8.5 | 0.64 | 1.41 |
| #5 | NF09 | Erzincan, 1992 | 6.7 | 2 | 0.43 | 0.85 |
| #6 | NF11 | Landers, 1992 | 7.3 | 1.1 | 0.71 | 0.95 |
| #7 | NF13 | Northridge, 1994, Rinaldi | 6.7 | 7.5 | 0.89 | 1.38 |
| #8 | NF15 | Northridge, 1994, Olive View | 6.7 | 6.4 | 0.73 | 1.01 |
| #9 | NF17 | Kobe, 1995 | 6.9 | 3.4 | 1.09 | 1.68 |
| #10 | NF19 | Kobe, 1995, Takatori | 6.9 | 4.3 | 0.79 | 1.70 |
| #11 | NF21 | Elysian Park 1 | 7.1 | 17.5 | 0.86 | 1.01 |
| #12 | NF23 | Elysian Park 2 | 7.1 | 10.7 | 1.80 | 3.16 |
| #13 | NF25 | Elysian Park 3 | 7.1 | 11.2 | 1.01 | 1.93 |
| #14 | NF27 | Elysian Park 4 | 7.1 | 13.2 | 0.92 | 2.40 |
| #15 | NF29 | Elysian Park 5 | 7.1 | 13.7 | 1.16 | 3.11 |
| #16 | NF31 | Palos Verdes 1 | 7.1 | 1.5 | 0.97 | 2.71 |
| #17 | NF33 | Palos Verdes 2 | 7.1 | 1.5 | 0.97 | 2.64 |
| #18 | NF35 | Palos Verdes 3 | 7.1 | 1.5 | 0.87 | 2.15 |
| #19 | NF37 | Palos Verdes 4 | 7.1 | 1.5 | 0.79 | 1.71 |
| #20 | NF39 | Palos Verdes 5 | 7.1 | 1.5 | 0.92 | 2.26 |

Table 1: List of the imposed near-fault accelerograms.

Regarding dynamic analysis, the computational efficient Fast-Nonlinear Analysis (FNA) is used in the present investigation. According to Sorace and Terenzi [15], FNA is ideal for structural systems in which the main non-linear response is related to the base-isolation system, while the superstructure's response remains elastic. In addition, the imposed ground motions are scaled utilizing the incremental dynamic analysis (IDA) method [16]. Peak ground acceleration is selected for the scaling, as previous studies (e.g., [17]) have considered it as a reliable

intensity measure (IM) for liquid storage tanks. Furthermore, the damping is set as 5% for the ultimate limit state of the tank [18], while for the impulsive liquid component is equal to 2%.

In this work, the fragility curves estimation are based on the methodology of fragility function fitting provided by Baker [19]. They are computed in terms of SFPB maximum displacement limit (i.e., 0.305m) for the Maximum Credible Earthquake (MCE) with 2% probability of exceedance in 50 years. SFPB isolators are modeled in SAP2000 program using the "Friction isolator" non-linear link element, which is capable of representing the SFPB behavior in a realistic manner. Regarding viscous damper, the "Exponential Maxwell damper" element is used, as it is capable of simulating the operation of the supplemental device. Linear viscous damper are selected, since the use of non-linear dampers does not affect considerably the results [20].

## 4 MULTI-OBJECTIVE OPTIMIZATION FORMULATION

In general, multi-objective optimization approaches can be more suitable than single-objective formulations, as the majority of real-life problems includes more than one design objectives. When considering competitive objective functions, a set of Pareto optimal solutions can be derived. Therefore, the selection among these solutions is achieved, by suitable trade-offs among the objectives, i.e., proper weight factors can be assigned to each optimization criterion and classify some Pareto solutions as more "attractive" to others. Consequently, the selection among Pareto results, as well as the use of multi-objective optimization approaches can be significantly beneficial in achieving cost-efficient design of hybrid isolation systems [9].

In the present investigation the multi-objective genetic algorithm (MOGA) is used, which is applied utilizing MATLAB optimization toolbox [14]). More specifically, two multi-objective optimization formulations, namely MOGA1 and MOGA2, are presented for the determination of the optimum parameters of the hybrid-isolation system. MOGA1 and MOGA2 include three and four objective functions respectively, since in MOGA2 the SFPB cost function is added in the formulation of MOGA1. The initial setup parameters of MOGA are presented in Table 2. The results are related to friction coefficient, radius of curvature, and damping coefficient for the two tanks. Regarding the design variables for SFPB isolators, the friction coefficient ranges from 0.01 to 0.12, and the radius of curvature ranges from 0.2032m to 6.0452m. Furthermore, following the recommendations of Providakis [11], the supplemental viscous damping ranges from 5% to 30%.

| Parameter | Selected Value / Function |
|---|---|
| Population size | 200 |
| Creation function | Constraint dependent |
| Mutation function | Constraint dependent |
| Selection | Tournament |
| Crossover fraction | 0.8 |
| Maximum generations | 2000 |

Table 2: Setup parameters of MOGA.

Regarding the objective functions, the first is related to damping. In particular, the integration of Equation (2) (isolator effective stiffness, $K_{eff}$ [N/m]) with Equation (3) (damping coefficient, $c_{VD}$ [Ns/m]):

$$K_{eff} = \frac{W}{R} + \mu \cdot \frac{W}{D} \tag{2}$$

$$c_{VD} = 2 \cdot \xi \cdot \sqrt{K_{eff} \cdot m} \tag{3}$$

leads to Equation (4) that describes the first objective function to be maximized [11]:

$$c_{VD} = 2 \cdot \xi \cdot \sqrt{\left(\frac{W}{R} + \mu \cdot \frac{W}{D}\right) \cdot m} \tag{4}$$

where $\xi$ is the supplemental viscous damping [%], $W$ denotes the weight of the tank [N], $\mu$ is the friction coefficient, $D$ refers to the maximum bearing displacement [m], $R$ denotes the radius of curvature [m] and, $m$ is the tank-liquid mass [kg].

In addition, the minimization of accelerations, $a$ [m/s$^2$], transmitted to the superstructure sets the second objective function [21]:

$$a = \left(\frac{D}{R} + \mu\right) \cdot g \tag{5}$$

where $g$ is the gravity of the Earth [m/s$^2$]. The minimization of maximum velocities developed at the SFPB devices, $v_{max}$ [m/s] is the aim of the third objective function [22]:

$$v_{max} = \frac{D}{\sqrt{\frac{1}{g \cdot \left(\frac{1}{R} + \frac{\mu}{D}\right)}}} \tag{6}$$

which is derived by combining Equations (7) and (8):

$$v_{max} = \frac{2 \cdot \pi \cdot D}{T_{SFPB}} \tag{7}$$

$$T_{SFPB} = 2 \cdot \pi \cdot \sqrt{\frac{1}{g \cdot \left(\frac{1}{R} + \frac{\mu}{D}\right)}} \tag{8}$$

where $T_{SFPB}$ represents the isolation period of SFPB isolators.

Lastly, the cost of SFPB isolators constitutes the fourth objective function, which is included only in the case of MOGA2 formulation [23]:

$$c = \exp\big(a(R) \cdot (D - 100)\big) \tag{9}$$

where, $a(R)$=0.0002·$R^2$-0.0014·$R$+0.0056. The aim of this criterion is to examine the impact of the incorporation of the significant parameter of isolators cost in the multi-objective optimization formulation.

**Constraint 1.** The isolators damping, $\beta_{eff}$, refers to the first constraint. In addition, damping should be within certain limits following the recommendations of seismic provisions [24]:

$$\beta_{eff} = \frac{2 \cdot \mu}{\pi \cdot D_D + \mu} \text{ and } 0.2 \leq \beta_{eff} \leq 0.3 \tag{10}$$

where $D_D$ is the isolator design displacement, (equal to 0.1m), based on Eurocode 8 guidelines [25]. By analyzing the lower and the upper bounds in Equation (10), the following two constraints are derived:

$$\beta_{eff} \leq 0.3 \;\Rightarrow\; \frac{2 \cdot \mu}{\pi \cdot \left(\frac{D_D}{R} + \mu\right)} \leq 0.3 \;\Rightarrow\; \mu - \frac{0.3 \cdot \pi \cdot D_D}{R \cdot (2 - 0.3 \cdot \pi)} \leq 0 \tag{11}$$

$$\beta_{eff} \geq 0.2 \;\Rightarrow\; \frac{2\cdot\mu}{\pi\cdot\left(\frac{D_D}{R}+\mu\right)} \geq 0.2 \;\Rightarrow\; \frac{0.2\cdot\pi\cdot D_D}{R\cdot(2-0.2\cdot\pi)} - \mu \leq 0 \tag{12}$$

**Constraint 2.** The period of the isolated superstructure is the second constraint of the optimization formulation:

$$T_{iso} = 2\cdot\pi\sqrt{\frac{1}{g\cdot\left(\frac{1}{R}+\frac{\mu}{D}\right)}} \text{ and } 2\ s \leq T_{iso} \leq 3\ s \tag{13}$$

which as previously is transformed into two constraints:

$$T_{iso} \geq 2\ s \Rightarrow \mu + D\cdot\left(\frac{1}{R} - \frac{\pi^2}{g}\right) \leq 0 \tag{14}$$

$$T_{iso} \leq 3\ s \Rightarrow D\cdot\left(\frac{1}{0.228\cdot g} - \frac{1}{R}\right) - \mu \leq 0 \tag{15}$$

**Constraint 3.** Lastly, the third constraints is related to the re-centering capability of SFPB isolators [26]:

$$\mu - \frac{D}{R} \leq 0 \tag{16}$$

## 5 RESULTS

### 5.1 MOGA1 Optimization results

In this section, the results of MOGA1 approach are briefly presented. In particular, the 3D Pareto front results are depicted in Figure 2. In addition, four optimum design (OD) levels (OD1, OD2, OD3, OD4) are selected to investigate the impact of the optimized hybrid isolation approach on the seismic response of squat and slender tanks. More specifically, OD1 and OD3 focus on optimizing the criterion related to acceleration and damping, respectively. Furthermore, OD2 and OD4 refer to two more balanced optimal solutions. Figure 2 highlights more clearly the differences among the selected OD solutions, while Table 3 presents the design variable values as well as the three objective functions MOGA1. Notable variations can be observed among the Pareto results of both tanks, which affect the isolation and superstructure performance.

| | | $\mu$ | $R$ [m] | $\xi$ [%] | $c_{VD}$ [kNs/m] | $v_{max}$ [m/s] | $a$ [m/s$^2$] |
|---|---|---|---|---|---|---|---|
| Squat tank | OD1 | 0.037 | 2.72 | 11 | 167.61 | 0.14 | 1.46 |
| | OD2 | 0.041 | 1.75 | 16.5 | 280.12 | 0.12 | 2.11 |
| | OD3 | 0.047 | 1.31 | 30 | 566.67 | 0.1 | 2.75 |
| | OD4 | 0.044 | 2.28 | 25 | 408.62 | 0.13 | 1.75 |
| Slender tank | OD1 | 0.038 | 2.78 | 9 | 110.62 | 0.14 | 1.45 |
| | OD2 | 0.05 | 1.89 | 12 | 170.30 | 0.12 | 2.07 |
| | OD3 | 0.046 | 1.22 | 28 | 431.87 | 0.1 | 2.9 |
| | OD4 | 0.040 | 1.60 | 26 | 361.06 | 0.11 | 2.26 |

Table 3: Optimization results of MOGA1 selected solutions.

Regarding fragility curves, Figure 3 presents the results for each tank in terms of isolators' displacement capacity. More specifically, the highest probabilities of exceedance for squat and slender tanks are presented by OD1 design, while slightly better results are produced by OD2.

It can be noticed that the best fragility results of the optimized hybrid schemes are derived for the OD3 design. In particular, the probabilities of exceedance – especially for PGA from 0.4g to approximately 1g – are significantly lower compared to the other two approaches for both tank slenderness ratios. In addition, quite different fragility results are obtained for OD4, as the probability of exceedance is higher for PGA from 0 to 0.3g, while fragility results become progressively better than OD1, OD2 and OD3 for high PGA levels.

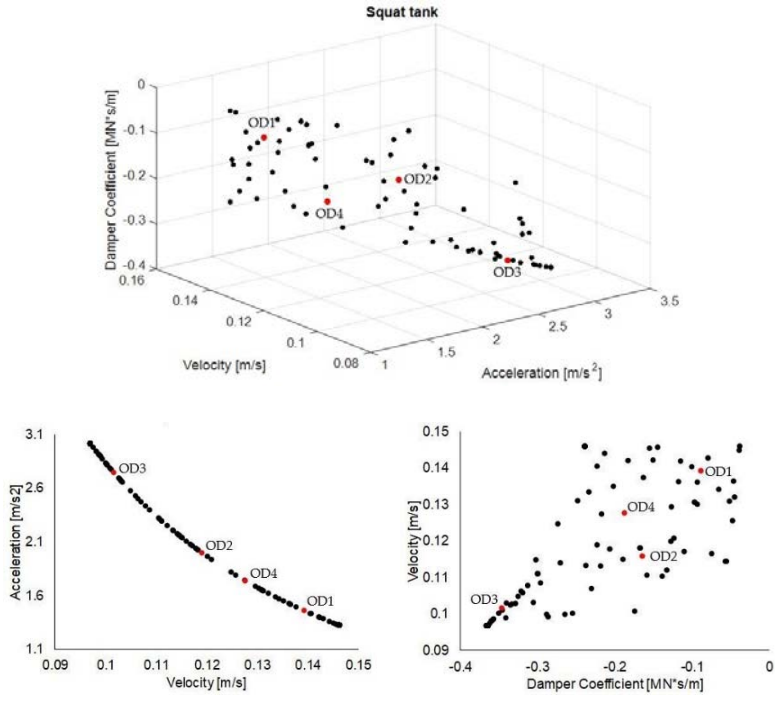


(a)

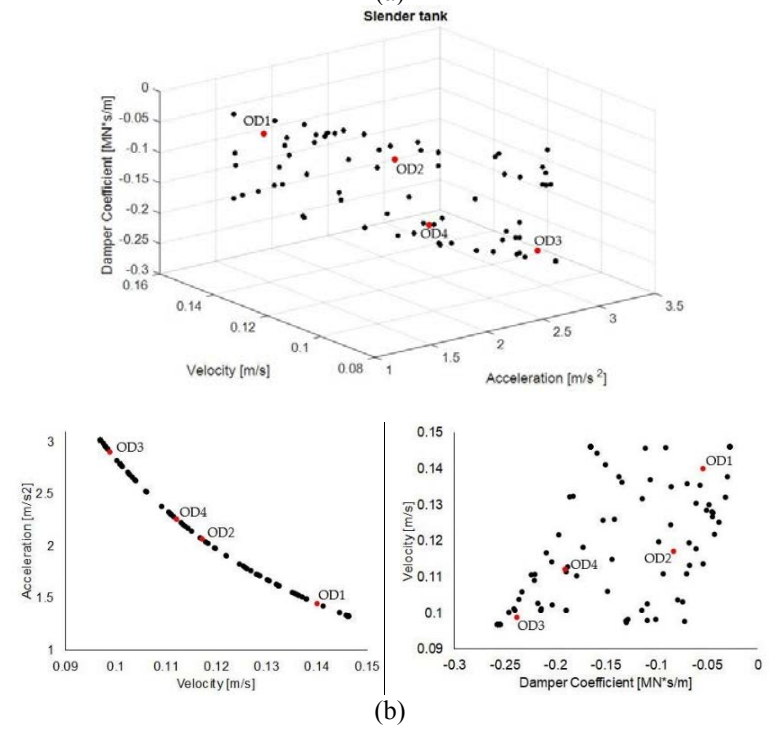


(b)

Figure 2: MOGA1 three- and two-dimensional representation of Pareto front results for: (a) the squat and (b) the slender tank.

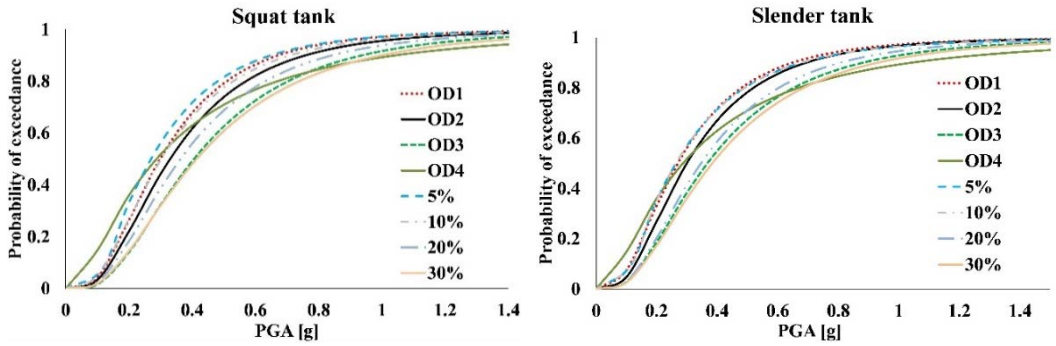


(a) (b)

Figure 3: Fragility curves derived from MOGA1 designs for: (a) the squat and (b) the slender tank.

Figure 3 also illustrates the fragility curves of conventionally designed hybrid isolated storage tanks presented in authors' previous study [27]. The comparison with the results derived from optimized configurations reveals that OD3 design presents almost identical fragility curves with the case of 30% supplemental damping for both tank slenderness ratios. This finding validates the main goal of OD3 design, which prioritizes damping maximization as close to the upper bound (i.e., 30%) as possible. Regarding slender tank (Figure 3b) the 20% curve is almost identical to OD3 and 30% curves. In addition, similar results are observed for 5%, 10% and OD2, which forms a group of two sets of results.

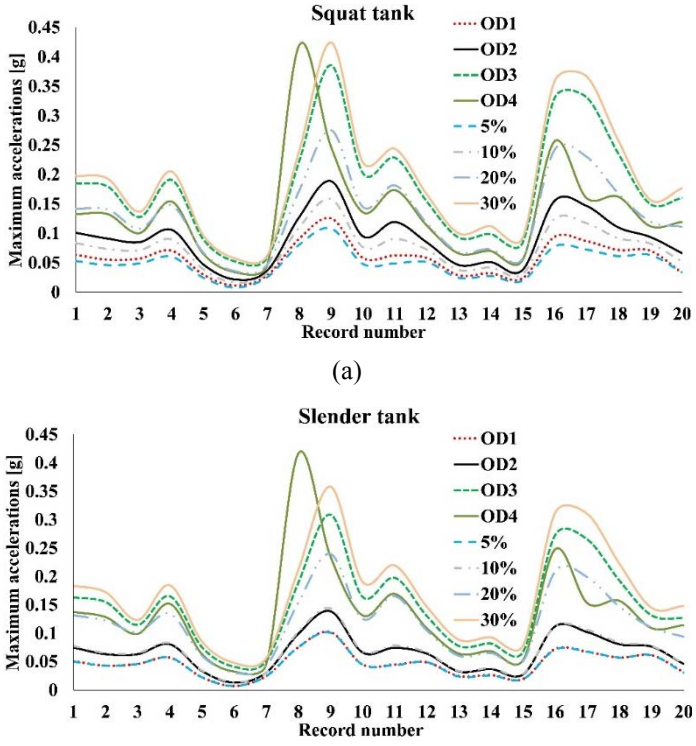


(a)

(b)

Figure 4: Base acceleration values derived from MOGA1 solutions for: (a) the squat and (b) the slender tank.

The accelerations transmitted to the superstructure are compared in Figure 4. As aforementioned, accelerations are significantly reduced due to the presence of the base-isolation combined with supplemental dampers. It should be noted that the results presented for all the examined optimized, as well as conventional hybrid designs, correspond to the maximum imposed values for every excitation. Consequently, it is shown that the frequency content of each

near-fault excitation, has significant impact on tank base accelerations depending also on the selected Pareto solution. In particular, OD1 design presents the lowest acceleration values, while slightly higher accelerations are exhibited in the case of OD2. Moreover, OD3 presents notably higher values for certain accelerograms. High acceleration results are obtained for OD4 solution for both squat and slender tanks, especially for accelerogram #8 (i.e., NF15 – Northridge record). When compared to conventional supplemental viscous damping designs, OD3 results present similar values with conventional design results with 30% supplemental damping. On the other hand, OD1 results are identical to 5% supplemental damping (i.e., the lowest level) for both tank slenderness ratios.

### 5.2 MOGA2 Optimization results

As aforementioned, four objective functions are included in the proposed MOGA2 approach. More specifically, in addition to the three objective functions of MOGA1, the cost function is added to enhance the cost-effectiveness of the multi-objective formulation. Table 4 and Figure 5 present the Pareto front results divided into three zones (low, medium, upper) for a better representation of the solutions of such complex multi-objective implementation. As previously, several solutions are selected and compared in terms of fragility curves and superstructure accelerations. More specifically, three optimized solutions are selected for the low (LL, LM, and LR) and medium (ML, MM, and MR) zone, and two for the upper zone (HL and HR).

| | Optimized Level | $\mu$ | $R$ [m] | $\xi$ [%] | $c_{VD}$ [kNs/m] |
|---|---|---|---|---|---|
| Squat tank | LL | 0.027 | 2.52 | 12 | 171.42 |
| | LM | 0.028 | 1.98 | 23.9 | 362.91 |
| | LR | 0.042 | 1.66 | 29.6 | 512.33 |
| | ML | 0.045 | 2.27 | 7.2 | 118.69 |
| | MM | 0.051 | 1.90 | 22.3 | 394.83 |
| | MR | 0.056 | 1.39 | 26.3 | 512.90 |
| | HL | 0.065 | 1.48 | 20.2 | 219.98 |
| | HR | 0.064 | 1.45 | 11 | 404.61 |
| Slender tank | LL | 0.025 | 2.76 | 11 | 122.50 |
| | LM | 0.036 | 2.04 | 24.6 | 313.26 |
| | LR | 0.036 | 1.61 | 30 | 406.03 |
| | ML | 0.044 | 2.12 | 19 | 253.57 |
| | MM | 0.052 | 1.73 | 25 | 365.71 |
| | MR | 0.044 | 1.29 | 23 | 345.73 |
| | HL | 0.056 | 1.22 | 30 | 387.98 |
| | HR | 0.061 | 1.35 | 24 | 485.19 |

Table 4: Optimization results of MOGA2 selected solutions.

Figure 6 depicts the fragility curves of the selected MOGA2 designs, in which significant differences are observed depending on tank slenderness ratio and the selected Pareto solution. In particular, the squat tank results present more scattered curves, and the best fragility results derive from LR and MR designs (Figure 6a). In contrast, the slender tank fragility curves exhibit a quite different behavior for the same designs (Figure 6b). In addition, a comparison between two Pareto solutions derived from the two multi-objective optimization approaches are presented in Figure 7. A similar trend can be observed, as OD3 design produces better fragility

results for PGA less than 0.6g and 0.5g for the squat and the slender tank, respectively. On the other hand, LR presents slightly better results for higher PGA levels. This is an indication that MOGA2 approach is preferable for high seismic intensity levels, as safer and more cost-efficient solutions are derived. Regarding base accelerations, Figure 8 illustrates the obtained results for the selected MOGA2 designs. Figure 8a refers to squat tank and it can be seen that ML and LL designs produce the lowest acceleration results, while LL, ML and LM solutions present the lowest values in the case of the slender tank, as presented in Figure 8b.

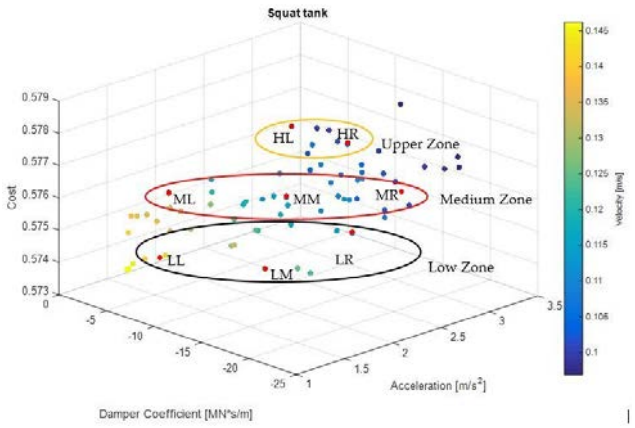


(a)

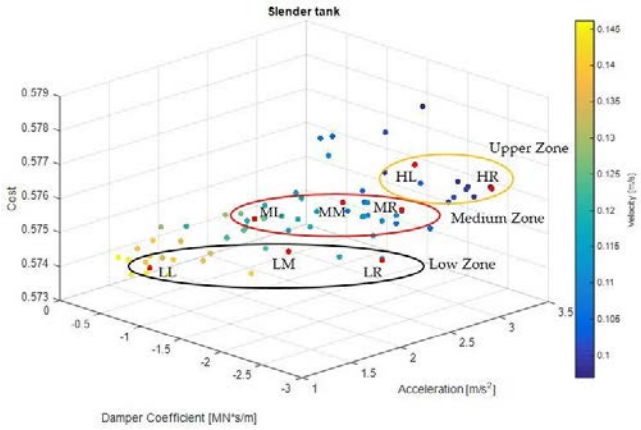


(b)

Figure 5: MOGA2 Pareto front results for: (a) the squat and (b) the slender tank.

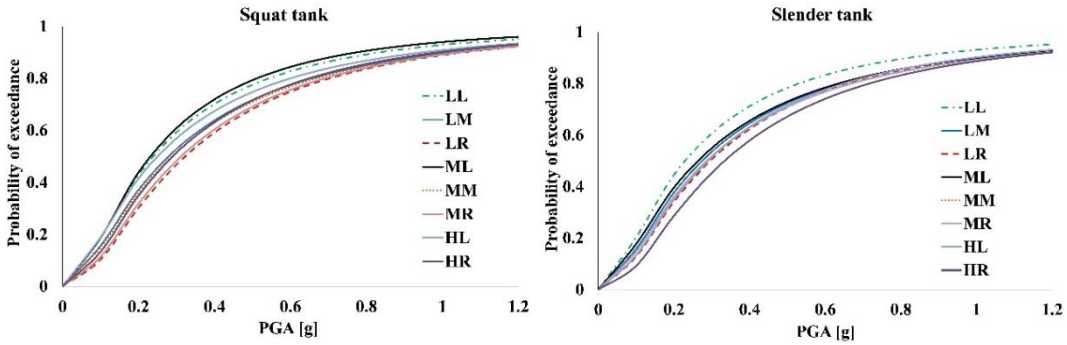


(a) (b)

Figure 6: Fragility curves derived from MOGA1 designs for: (a) the squat and (b) the slender tank.

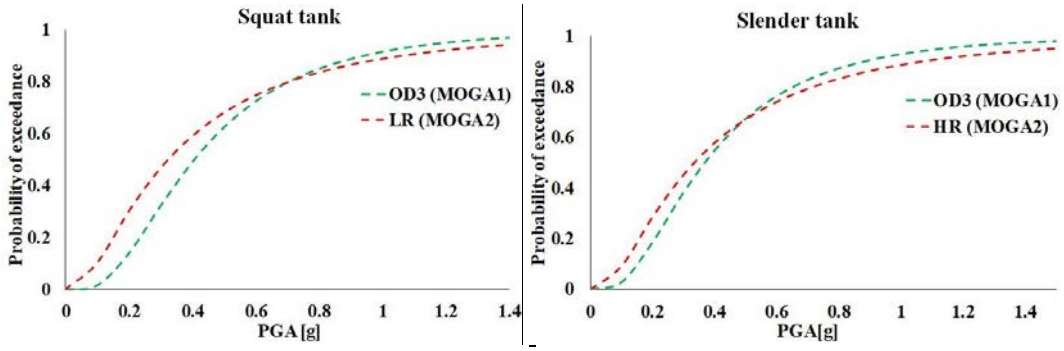


Figure 7: MOGA1 and MOGA2 fragility curves comparison for: (a) the squat and (b) the slender tank.

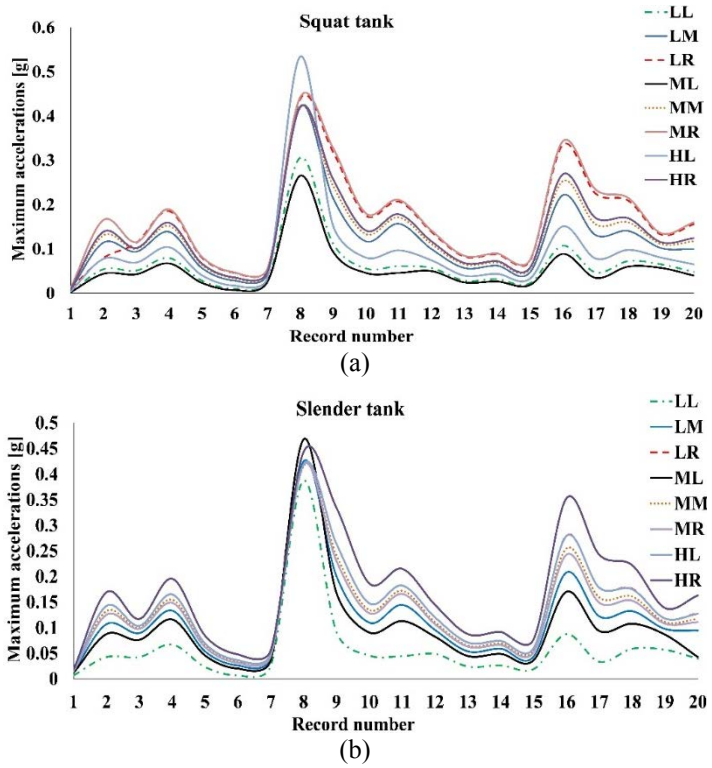


Figure 8: Base acceleration values derived from MOGA2 solutions for: (a) the squat and (b) the slender tank.

## 6 CONCLUSIONS

In this work, two novel multi-objective optimization formulations have been presented to improve the seismic performance of hybrid-isolated liquid storage tanks. The examined squat and slender tanks have been equipped with SFPB isolators in combination with supplemental linear viscous dampers. The isolation system is optimized in an efficient multi-criteria manner. More specifically, the MOGA1 optimization formulation consists of three objective functions, while MOGA2 included an additional objective function related to SFPB cost. The design variables for both approaches are related to the friction coefficient, radius of curvature and the percentage of supplemental damping. In addition, the isolators effective period and damping, combined with the re-centering capability of friction devices are adopted as constraint functions.

An efficient multi-objective genetic algorithm (MOGA) optimizer has been applied to perform optimization calculations for both formulations. The results have been presented in terms of isolators fragility curves and accelerations transmitted to the superstructure for both tank

slenderness ratios. Moreover, comparisons have been made with conventionally designed hybrid systems (i.e., without performing any optimization). The following conclusions can be derived from the present investigation:

- MOGA constitutes an efficient optimization method for complex real-life problems, such as base-isolated liquid storage tanks with supplemental damping.
- Regarding MOGA1 approach, the best fragility results derived from OD3 design, while OD1 produced the lowest base accelerations. OD2 design is selected as the most efficient approach due to the optimal balance between fragility results and the transmitted base accelerations.
- Regarding MOGA2 approach the best fragility results have been derived from the HR design, while LL presented the lowest accelerations transmitted to the superstructure. However, the most efficient approach considering the best fragility curves and the lower base accelerations is the LM design.
- The comparison of the proposed MOGA1 and MOGA2 optimization approaches has shown that MOGA2 is slightly superior to MOGA1 for high seismic intensity levels (i.e., greater than 0.5g) and vice versa.

## REFERENCES

[1] M. Farajian, N. Saeed, W. Kang, Seismic vulnerability assessment of base isolated liquid storage tanks under near-fault ground motions. *Structures,* **43**, 1901-1912, 2022.

[2] D. De Domenico, E. Gandelli, V. Quaglini, Adaptive isolation system combining low-friction sliding pendulum bearings and SMA-based gap dampers. *Engineering Structures*, **212**, 110536, 2020.

[3] S, Pourzeynali, M. Zarif, Multi-objective optimization of seismically isolated high-rise building structures using genetic algorithms. *Journal of Sound and Vibration*, **311**, 1141–1160, 2008.

[4] O.E. Ozbulut, M. Bitaraf, S. Hurlebaus, Adaptive control of base-isolated structures against near-field earthquakes using variable friction dampers. *Engineering Structures*, **33** (12), 3143–3154, 2011.

[5] N. Fallah, G. Zamiri, Multi-objective optimal design of sliding base isolation using genetic algorithm. *Scientia Iranica*, **20** (1), 87–96, 2013.

[6] D.Z. Labaf, M. De Angelis, M. Basili, Multi-objective optimal design and seismic assessment of an inerter-based hybrid control system for storage tanks. *Bulletin of Earthquake Engineering*, **43**, 1091–1099, 2022.

[7] K. Bakalis, M. Fragiadakis, D. Vamvatsikos, Surrogate modeling for the seismic performance assessment of liquid storage tanks. *Journal of Structural Engineering*, **143** (4), 04016199, 2017.

[8] E. Güler, C. Alhan, Performance limits of base-isolated liquid storage tanks with/without supplemental dampers under near-fault earthquakes. *Structures*, **33**, 355-367, 2021.

[9] A. Tsipianitis, Y. Tsompanakis, Multi-objective optimization of base-isolated tanks with supplemental linear viscous dampers. *Infrastructures,* **7**, 157, 2022.

[10] M. Lafontaine, O. Moroni, M. Sarrazin, P. Roschke, Optimal control of accelerations in a base-isolated building using magneto-rheological dampers and genetic algorithms. *Journal of Earthquake Engineering*, **13** (8), 1153–1171, 2009.

[11] C.P. Providakis, Effect of supplemental damping on LRB and FPS seismic isolators under near-fault ground motions. *Soil Dynamics and Earthquake Engineering*, **29** (1), 80–90, 2009.

[12] A.W. Taylor, Response control systems in the United States and lessons learned from the Tohoku earthquake. *International Symposium on Engineering Lessons Learned from the 2011 Great East Japan Earthquake*, Tokyo, Japan, 1087-1098, 2012.

[13] CSI Computers and Structures Inc. *SAP2000 Version 20. Integrated Software for Structural Analysis and Design, Analysis Reference Manual*; Computers and Structures Inc.: Berkeley, CA, 2017.

[14] Mathworks, Inc. *MATLAB & Optimization Toolbox R2015a*. Natick. M.A., USA, 2015.

[15] S. Sorace, G. Terenzi, Analysis and demonstrative application of a base isolation/supplemental damping technology. *Earthquake Spectra*, **24** (3), 775–793, 2008.

[16] D. Vamvatsikos, C. Allin Cornell, Incremental dynamic analysis. *Earthquake Engineering and Structural Dynamics*, **31** (3), 491–514, 2002.

[17] M. D-Amico, N. Buratti, Observational seismic fragility curves for steel cylindrical tanks. *Journal of Pressure Vessel Technology*, **141** (1), 2019.

[18] CEN. *Eurocode 8 - Design of Structures for Earthquake Resistance - Part 4: Silos, Tanks and Pipelines EN 1998-4*; European Committee for Standardization, Brussels, Belgium, 2006.

[19] J.W. Baker, Efficient analytical fragility function fitting using dynamic structural analysis. *Earthquake Spectra*, **31** (1), 579–599, 2015.

[20] E.D. Wolff, C. Ipek, M.C. Constantinou, M. Tapan, Effect of viscous damping devices on the response of seismically isolated structures. *Earthquake Engineering and Structural Dynamics*, **44** (2), 185–198, 2015.

[21] A. Tsipianitis, Y. Tsompanakis, Optimizing the seismic response of base-isolated liquid storage tanks using swarm intelligence algorithms. *Computers and Structures*, **243**, 2021.

[22] S. Barone, G.M. Calvi, A. Pavese, Experimental dynamic response of spherical friction-based isolation devices. *Journal of Earthquake Engineering*, **23** (9), 1465–1484, 2019.

[23] C. Bucher, Analysis and design of sliding isolation pendulum systems. *IABSE Symposium Report*, 104 (5), 1–8, 2015.

[24] C. Yenidogan, M.A. Erdik, Comparative evaluation of design provisions for seismically isolated buildings. *Soil Dynamics and Earthquake Engineering*, **90**, 265–286, 2016.

[25] CEN. *Eurocode 8 - Design of Structures for Earthquake Resistance - Part 1: General rules, seismic actions and rules for buildings EN 1998-1*; European Committee for Standardization, Brussels, Belgium, 2004.

[26] M.J.N. Priestley, G.M. Calvi, M.J. Kowalsky, *Displacement-based seismic design of structures*. IUSS Press, 2007

[27] A. Tsipianitis, Y. Tsompanakis, Improving the seismic performance of base-isolated liquid storage tanks with supplemental linear viscous dampers. *Earthquake Engineering and Engineering Vibration*, **21** (1), 269–282, 2022.